Whistler-mode waves excited by anisotropic hot electrons with a drift velocity in Earth's magnetosphere: Linear theory

Kai Fan[1,2], Jicheng Sun[3], and Jun Guo[4*]

[1]CAS Key Laboratory of Geospace Environment, Department of Geophysics and Planetary Science, University of Science and Technology of China, Hefei 230026, China

[2]Shandong Provincial Key Laboratory of Optical Astronomy and Solar-Terrestrial Environment，Shandong University, Weihai, 264209, China

[3]Physices Department, Auburn University, Auburn, Alabama, USA

[4] College of Mathematics and Physics, Qingdao University of Science and Technology, Qingdao, 266061, China

[*]Email: guoj2005@163.com

Abstract

With a linear theoretical model, we have investigated the properties of whistler waves excited by anisotropic hot electrons with a drift velocity, which is usually neglected in previous studies. It is found that a finite drift velocity can significantly change the properties of excited whistler waves, resulting in distinct properties for parallel and antiparallel propagating waves. In the high-beta regime, as the drift velocity increases, the frequency of parallel propagating whistler waves increases, while that of antiparallel propagating waves is found to decline. So parallel and antiparallel propagating whistler waves appear in different frequency bands. However, the growth rate of parallel wave is always smaller than that of antiparallel wave, and falls below $10^{-2}\Omega_e$ for large drift velocities ($v_d/v_{th} > 1.5$), in which case the parallel wave may be too weak to be observed. Generally, the growth rate of whistler waves in both directions is enhanced with the increasing anisotropy or proportion of hot electrons. In the low-beta regime, the trends of the frequency and linear growth rate of excited whistler waves are quite similar to those in the high-beta regime. But, with the increase of the drift velocity, the wave normal angle of parallel propagating whistler waves gradually declines until reaching zero, while that of antiparallel propagating waves continues to increase. Our study may help people to better understand various whistler-mode spectra observed in the Earth's magnetosphere.

1. Introduction

Whistler-mode waves, also known as chorus waves, are one of the most intense natural emissions at frequencies between 0.1 and 0.8f_{ce} (f_{ce} is the equatorial electron gyrofrequency) in the Earth's magnetosphere (Burtis and Helliwell, 1969; Tsurutain & Smith, 1974; Li et al., 2012). They have received much attention due to their key role in controlling electron dynamics in the Earth's Van Allen radiation belt. Chorus waves have been commonly believed to account for both the precipitation of low-energy (0.1-30keV) electrons into atmosphere (Thorne et al., 2010; Ni et al., 2011; Nishimura et al., 2013) and the dominant source of relativistic electrons (~MeV) in the heart of radiation belt during geoactive periods (Summers et al., 2002; Reeves et al., 2013; Thorne et al., 2013). In the spectrogram, whistler-mode chorus waves are typically divided into two separated bands by a power gap around 0.5f_{ce} (Meredith et al., 2001; Ratcliffe and Watt, 2017): lower band (0.1f_{ce}-0.5f_{ce}) and upper band (0.5f_{ce}-0.8f_{ce}). Much effort has been made to understand the formation of the power gap around 0.5f_{ce} (Omura et al., 2009; Fu et al., 2015; Gao et al., 2016a, 2017, 2018, 2019), but there is still no consensus reached on this issue. The majority of whistler-mode chorus waves in Earth's magnetosphere are quasi-parallel with wave normal angle (WNA) smaller than 30° (Li et al., 2011), while there is also a significant population of very oblique waves with WNA near the resonant angle (Li et al., 2011; Gao et al., 2016b). The main source region of whistler-mode waves is located at the magnetic equator and just extends to several degrees of magnetic latitude (Lauben et al., 2002; Santolik et al., 2005).

It is widely accepted that whistler-mode waves in the Earth's magnetosphere extract free energy from energetic electrons injected from plasma sheet during geoactive periods (Li et al., 2010; Gao et al., 2014). These tens of keV electrons usually have significant temperature anisotropies with $T_\perp > T_\parallel$, which are unstable to the whistler anisotropy instability (Lu et al., 2004, 2010; Santolik et al., 2010; Liu et al., 2011; Omura and Nunn, 2011; Gary et al., 2011; Ke et al., 2017). Hereafter, the subscripts $\perp$ and $\parallel$ denote the directions perpendicular and parallel to the background magnetic field. In previous studies, this energy source is often modeled as a single bi-Maxwellian distribution in velocity space without the bulk velocity. In this scenario, whistler-mode waves with parallel and anti-parallel propagating directions are simultaneously excited in the source region and have the same amplitude, which has been supported by both the linear theory and PIC simulations (Gary et al., 2011; An et al., 2017; Chen et al., 2018; Fan et al., 2019). As a result, the presence of mixed Poynting flux directions of whistler-mode chorus waves becomes a common method to determine their source region from satellite observations (LeDocq et al., 1998; Santolik et al., 2003). Besides, the wave normal angle of excited whistler-mode waves is mainly controlled by the parallel plasma beta ($\beta_\parallel$) of anisotropic energetic electrons (Gary et al., 2011; Yue et al., 2016; An et al., 2017; Fan et al., 2019). Generally, in the high-beta ($\beta_\parallel \geq 0.025$) regime, the WNA of whistler mode with the largest linear growth rate is always zero. While, in the low-beta ($\beta_\parallel \leq 0.025$) regime, the WNA of the most unstable whistler mode will become very large ($> \sim 40^\circ$).

Recent observations from THEMIS satellite have revealed that both

quasi-parallel and oblique whistler-mode chorus waves are usually detected along with a beam-like electron population in the Earth's magnetosphere (Chen et al., 2019). This implies that the bi-Maxwellian electron distribution with a drift velocity along the background magnetic field is a better model describing anisotropic energetic electrons. With a theoretical model, Mourenas et al. (2015) proposed that very oblique (WNA$\approx arccos^{-1} f/f_{ce}$) lower-band whistler waves can be generated by anisotropic electron beam through a combination of cyclotron resonance and Landau resonance. This potential mechanism has been supported by a statistical study on very oblique chorus waves (Gao et al., 2016b). However, the effect of a finite drift velocity of anisotropic energetic electrons on excited whistler waves is still not fully understood.

In this paper, we have comprehensively studied the properties of whistler waves excited by anisotropic electrons with a finite drift velocity along the background magnetic field with a linear theoretic model. Especially, we focus on the effects of the drift velocity on the linear growth rate, wave frequency, and WNA of excited whistler waves in both high-beta and low-beta regimes. It is found that a modest drift velocity can significantly change the properties of excited whistler waves, but the changes are quite different in two propagating directions, i.e., parallel and anti-parallel to the background magnetic field.

The rest of this paper is structured as follows. Section 2 describes the linear theoretical model used in this study, and theoretical results for both high-beta and low-beta regimes are presented in Section 3. Section 4 is a summary of principal

results.

2. Linear theoretical model

We have investigated the effects of the drift velocity on whistler-mode waves excited by anisotropic hot electrons using the linear theory. The WHAMP (Waves in Homogeneous Anisotropic Magnetized Plasma) model (Ronnmark, 1982), which can be easily accessed on https://github.com/irfu/whamp, is utilized to calculate the dispersion relation of whistler mode and associated linear growth rates. This code has been widely used in previous works (Xiao et al., 2007; Chen et al., 2018; Denton, 2018; Fan et al., 2019).

In this study, the background magnetic field B_0 and plasma density n_{total} are assumed as 80 nT and 1.0 cm^{-3}, meaning the ratio between plasma frequency and gyrofrequency (ω_{pe}/Ω_e) is about 4, which is a typical value in the source region of whistler-mode waves (Gao et al., 2014). In this model, there are three species in the plasma, such as cool protons, cool electrons, and hot electrons, which are denoted by subscripts “p”, “c”, and “h”, respectively. The background cool protons and cool electrons both satisfy the Maxwellian velocity distribution and have the same temperature of 1 eV. The hot electrons are the source of free energy to excite whistler waves, which are described as a drifting bi-Maxwellian distribution:

$$f_h(v_\perp, v_\parallel) = \frac{n_h}{(2\pi)^{3/2} v_{th}^3} exp\left[-\frac{(v_\parallel - v_{dh})^2}{2v_{th}^2}\right] \frac{T_{\parallel h}}{T_{\perp h}} exp\left[-\frac{v_\perp^2}{2(T_{\perp h}/T_{\parallel h})v_{th}^2}\right],$$

where n, v, and T represent the density, velocity, and temperature, respectively. The

v_{th} and v_d denote the parallel thermal velocity and drift velocity of hot electrons, respectively. Besides, the background magnetic field is along *z* axis, and the densities of three species satisfy $n_h + n_c = n_p = n_{total}$. Note that, to perform one linear theory calculation, we need to initialize some parameters in the WHAMP model, such as the density, parallel beta, anisotropy, and drift velocity of each component, and ω_{pe}/Ω_e.

3. Results

The parallel plasma beta $\beta_{||h}$ $(= 2\mu_0 n_{total} k_B T_{||h}/B_0^2)$ of hot electrons is a key parameter controlling the WNA of excited whistler-mode waves. Previous studies revealed that the whistler wave with the maximum growth rate undergoes a transition from parallel to oblique propagation at a critical value ($\sim$0.025) of $\beta_{||h}$ (Gary et al., 2011; Yue et al., 2016; An et al., 2017; Fan et al., 2019). Therefore, we have investigated the effects of drift velocity of hot electrons on excited whistler waves in these two regimes with the WHAMP model.

3.1 High-beta Regime: $\boldsymbol{\beta_{\|h} > 0.025}$

Since the linear growth rate of unstable whistler waves always peaks at the WNA of 0° in our considered cases, we only consider parallel and antiparallel propagating whistler waves in this regime. Figure 1 exhibits the frequency ω/Ω_e (black lines) and linear growth rate γ/Ω_e (red lines) of whistler waves as a function of parallel wave number $k_\| v_{th}/\Omega_e$ for two cases with different relative drift velocities: (a)

$v_d = 0$ and (b) $v_d = 1.0v_{th}$. In two cases, the parallel plasma beta $\beta_{||h}$, anisotropy $T_{\perp h}/T_{\parallel h}$, number density n_h/n_{total} of hot electrons are fixed as 0.32, 4, and 0.1, respectively. Hereafter, solid and dashed lines represent whistler waves that propagate parallel and antiparallel to the background magnetic field, respectively. Just as expected, without the drift velocity, the whistler waves driven by anisotropic hot electrons have the same dispersion relation and linear growth rate in parallel and antiparallel directions (Figure 1a). In Figure 1a, the frequency ω/Ω_e and linear growth rate γ/Ω_e of the most unstable whistler wave are 0.46 and 0.035 in both directions. However, when anisotropic electrons are given a drift velocity of $1.0v_{th}$ in Figure 1b, the properties of unstable whistler waves have changed significantly. For parallel propagating waves, the most unstable whistler mode now has a higher frequency of $0.61\Omega_e$ ($>0.5\Omega_e$) but a smaller linear growth rate of $0.019\Omega_e$. While, for antiparallel propagating waves, the most unstable whistler mode has a lower frequency of $0.3\Omega_e$ ($<0.5\Omega_e$) but a larger linear growth rate of $0.036\Omega_e$. As a result, there exist obvious differences between parallel and antiparallel propagating waves, making it very easy to distinguish them in the spectrogram. That is, parallel propagating whistler waves fall within upper band ($>0.5\Omega_e$) and have smaller amplitudes, but antiparallel propagating waves belong to lower band ($<0.5\Omega_e$) and have larger amplitudes.

The pitch-angle distribution of electrons for two cases are shown in Figure 2. The coded color denotes the velocity of electrons. As shown in Figure 2a, without the drift velocity of hot electrons, the phase space density (PSD) of electrons at a fixed

velocity exhibits a symmetric distribution about the pitch angle of 90°, and just peaks at 90° due to the temperature anisotropy. In Figure 2b, there is a drift velocity of $1.0v_{th}$ along the background magnetic field, so the pitch-angle distribution entirely move toward smaller pitch angles, making the profile of PSD becomes asymmetric. The maximum PSD is not at the pitch angle of 90° but shifts toward smaller pitch angles. And the peak of PSD of lower-energy electrons is farther away from 90° pitch angle. Therefore, the asymmetric pitch-angle distribution can be considered as an identity of drifting anisotropic electrons in observation data.

Figure 3 gives a summary plot, including the effects of drift velocity v_d/v_{th}, anisotropy $T_{\perp h}/T_{\parallel h}$, proportion n_h/n_{total} of hot electrons on the frequency ω_d/Ω_e (left column) and growth rate γ_d/Ω_e of most unstable whistler mode in both parallel (solid lines) and antiparallel (dashed lines) directions, respectively. Except the parameter of interest, such as v_d/v_{th}, $T_{\perp h}/T_{\parallel h}$, and n_h/n_{total}, other initial parameters are fixed as those in the case shown in Figure 1b. With the increase of drift velocity, as shown in Figure 1a, the frequency of parallel propagating whistler continuously increases, while that of antiparallel propagating whistler is found to decline. As a result, the parallel and antiparallel propagating whistler will be observed in upper and lower band in the spectrogram, respectively. And a power gap between them is naturally formed. However, the growth rate of parallel whistler is always smaller than that of antiparallel wave for nonzero drift velocities, and further smaller for a larger drift velocity (Figure 3b). It is worth mentioning, since the growth rate of parallel whistler is quite small ($\gamma_d/\Omega_e < 10^{-2}$) for a large drift velocity ($v_d/v_{th} >$

1.5), then the parallel wave may be too weak to be observed in such case.

With a fixed drift velocity of $1v_{th}$, the frequency difference between parallel and antiparallel propagating whistler waves seems to be independent on the anisotropy and proportion of hot electrons (Figures 3c and 3e). Generally, the growth rate of whistler waves in both directions will increase as the $T_{\perp h}/T_{\parallel h}$ or n_h/n_{total} increases (Figures 3d and 3f). However, there are still two things should be pointed out. Firstly, when the $T_{\perp h}/T_{\parallel h}$ is below ~2.5, the growth rate of parallel wave is somehow larger than that of antiparallel wave, but their growth rates become a very low level (Figure 3d). Then, if the n_h/n_{total} is reduced below ~5, there may be only lower-band (or antiparallel propagating) whistler waves excited in the system due to the low growth rate of parallel waves (Figure 3f).

3.2 Low-beta Regime: $\boldsymbol{\beta_{\parallel h} < 0.025}$

Figure 4 displays the frequency ω_m (black lines) and linear growth rate γ_m (red lines) as a function of WNA θ for two cases with different relative drift velocities: (a) $v_d = 0$ and (b) $v_d = 0.5v_{th}$. Here ω_m and γ_m denote the frequency and growth rate of whistler mode with the maximum linear growth rate at each WNA. In Figure 4a, similar to results in Figure 1a, parallel and antiparallel propagating whistler waves also have the same frequency and growth rate, but the linear growth rate peaks at the large WNA ($\sim 40^{\circ}$) in this low-beta regime. If given a drift velocity of $0.5v_{th}$ as shown in Figure 4b, the most unstable whistler wave in parallel direction will have the smaller WNA ($\sim 28^{\circ}$) and linear growth rate ($\sim 0.0094\Omega_e$) but

larger frequency, while that in antiparallel direction will have the larger WNA ($\sim 47^{\circ}$) and linear growth rate ($\sim 0.0135\Omega_e$) but lower frequency. In the same format as Figure 2, Figure 5 gives the pitch-angle distribution of hot electrons for above two cases. One this to keep in mind is that the pitch-angle distribution of hot electrons will become asymmetric in the presence of a finite drift velocity (Figure 5b).

In low-beta regime, we have investigated not only the effects of drift velocity, anisotropy, proportion of hot electrons on the frequency and growth rate of most unstable whistler mode in both directions but also the WNA, which are presented in Figure 6. Except the parameter of interest, such as v_d/v_{th}, $T_{\perp h}/T_{\parallel h}$, and n_h/n_{total}, other initial parameters are fixed as those in the case shown in Figure 4b. In Figures 1a-1c, for parallel propagating whistler wave (solid lines), as the drift velocity increases, the frequency increases but the growth rate and WNA decreases. But, the trend for antiparallel propagating whistler wave (dashed lines) is totally opposite. So the differences between parallel and antiparallel waves in frequency, growth rate, and WNA will become more significant with the increase of drift velocity. Specifically, with a finite drift velocity, the anisotropic hot electrons can simultaneously generate the quasi-parallel and very oblique whistler waves within the source region (Figure 6c). The frequency and wave normal angle of excited whistler waves seem to be independent on the $T_{\perp h}/T_{\parallel h}$ and n_h/n_{total} of hot electrons (Figures 6d, 6f, 6g, and 6i). But there is a clear trend that the growth rates of both parallel and antiparallel propagating whistler waves increase with the $T_{\perp h}/T_{\parallel h}$ or n_h/n_{total} (Figures 6e and 6h). It is found that the growth rate of antiparallel wave is always larger than that of

parallel waves, but their ratio nearly remains constant (Figures 6e and 6h).

4. Conclusion and Discussion

In this study, we have comprehensively investigated the properties of whistler waves excited by anisotropic hot electrons with a drift velocity with a linear theoretical model. We find that a finite drift velocity can significantly modulate the properties of excited whistler waves, but cause different effects on parallel and antiparallel propagating waves. In the high-beta regime, the WNA of most unstable whistler mode remains zero, irrespective of the drift velocity. As the drift velocity increases, the frequency of parallel propagating whistler wave increases, while that of antiparallel propagating wave is found to decline. As a result, parallel and antiparallel propagating whistler waves appear in the upper and lower bands, respectively. However, the growth rate of parallel wave is always smaller than that of antiparallel wave, and falls below $10^{-2}\Omega_e$ for large drift velocities ($v_d/v_{th} > 1.5$), in which case the parallel wave may be too weak to be observed. Generally, the growth rate of whistler waves in both directions will increase with the increasing anisotropy or proportion of hot electrons. In the low-beta regime, the trends of the frequency and linear growth rate of excited whistler waves are quite similar to those in the high-beta regime. But, with the increase of the drift velocity, the WNA of parallel propagating whistler waves gradually decline until reaching zero, while that of antiparallel propagating waves continues to increase.

In previous studies, the energy source that drives the excitation of whistler waves

in the inner magnetosphere is commonly modeled as energetic electrons satisfying the bi-Maxwellian velocity distribution (Santolik et al., 2010; Liu et al., 2011; Gary et al., 2011; Yue et al., 2016; An et al., 2017; Fan et al., 2019), and the frequency-time spectrogram is expected to be identical in parallel and antiparallel directions. However, according to our results, the parallel and antiparallel propagating whistler waves will exhibit quite different properties in the presence of the drift velocity of energetic electrons, such as the frequency, amplitude (or growth rate), and WNA. In the high-beta regime, the generated whistler waves can show up in different frequency bands (Figures 1 and 3), i.e., lower and upper bands, leaving a power gap between them. This could be another potential mechanism to explain the banded spectrum observed in magnetosphere. In the low-beta regime, both quasi-parallel and oblique whistler waves can be excited at the same time from one energy source (Figures 4 and 6). Besides, whistler waves are also frequently observed in association with magnetic reconnections at the magnetopause or magnetotail (Deng and Matsumoto, 2001; Wei et al., 2007; Huang et al., 2016; Cao et al., 2017; Wang et al., 2019), where the drift velocity of energized electrons is typically large. Therefore, our study may provide some new insights in understanding various whistler-mode spectra detected in the Earth's magnetosphere.

Acknowledgement

This work is supported by the Shandong Provincial National Natural Science Foundation (ZR2017MD012), and the Specialized Research Fund for Shandong

Provincial Key Laboratory. No simulation and observational data are used in this work.

References

An, X., C. Yue, J. Bortnik, V. Decyk, W. Li, and R. M. Thorne (2017), On the parameter dependence of the whistler anisotropy instability, J. Geophys. Res. Space Physics, 122, 2001–2009, doi:10.1002/2017JA023895.

Burtis, W. J., and R. A. Helliwell (1969), Banded chorus a new type of VLF radiation observed in the magnetosphere by OGO 1 and OGO 3. Journal of Geophysical Research, 74(11), 3002-3010. https://doi.org/10.1029/JA074i011p03002.

Cao, D., et al. (2017), MMS observations of whistler waves in electron diffusion region, Geophys.Res.Lett.,44, 3954-3962, doi:10.1002/2017GL072703.

Chen, H. Y., X. L. Gao, Q. M. Lu, J. C. Sun, and S. Wang (2018), Nonlinear evolution of counter-propagating whistler mode waves excited by anisotropic electrons within the equatorial source region: 1-D PIC simulations. Journal of Geophysical Research: Space Physics, 123, 1200 – 1207. https://doi.org/10.1002/2017JA024850.

Chen, R., X. L. Gao, Q. M. Lu, and S. Wang (2019), Unraveling the correlation between chorus wave and electron beam-like distribution in the Earth's magnetosphere. Geophysical Research Letters, 46, https://doi.org/10.1029/

2019GL085108.

Deng, X. H., and H. Matsumoto (2001), Rapid magnetic reconnection in the Earth's magnetosphere mediated by whistler waves, Nature, 410, 557–560, doi:10.1038/35069018.

Denton, R. E. (2018), Electromagnetic ion cyclotron wavefields in a realistic dipole field. Journal of Geophysical Research: Space Physics, 123, 1208 – 1223. https://doi.org/10.1002/2017JA024886.

Fan, K., X. L. Gao, Q. M. Lu, J. Guo, and S. Wang (2019), The effects of thermal electrons on whistler mode waves excited by anisotropic hot electrons: Linear theory and 2-D PIC simulations. Journal of Geophysical Research: Space Physics, 124. https://doi.org/10.1029/ 2019JA026463.

Fu, X., Z. Guo, C. Dong, and S. P. Gary (2015), Nonlinear subcyclotron resonance as a formation mechanism for gaps in banded chorus, Geophys. Res. Lett., 42, 3150-3159, doi:10.1002/2015GL064182.

Gao, X. L., W. Li, R. M. Thorne, J. Bortnik, V. Angelopoulos, Q. M. Lu, X. Tao, and S. Wang (2014), New evidence for generation mechanisms of discrete and hiss-like whistler mode waves. Geophysical Research Letters, 41, 4805 – 4811. https://doi.org/10.1002/2014GL060707.

Gao, X. L., Q. M. Lu, J. Bortnik, W. Li, L. J. Chen, and S. Wang (2016a), Generation

306 of multiband chorus by lower band cascade in the Earth's magnetosphere.
307 Geophysical Research Letters, 43, 2343–2350.
308 https://doi.org/10.1002/2016GL068313.

309 Gao, X., D. Mourenas, W. Li, A. V. Artemyev, Q. M. Lu, X. Tao, and S. Wang
310 (2016b), Observational evidence of generation mechanisms for very oblique
311 lower band chorus using THEMIS waveform data, J. Geophys. Res. Space
312 Physics, 121, 6732–6748.

313 Gao, X. L., Y. G. Ke, Q. M. Lu, L. J. Chen, and S. Wang (2017), Generation of
314 multiband chorus in the Earth's magnetosphere: 1-D PIC simulation.
315 Geophysical Research Letters, 44, 618–624.
316 https://doi.org/10.1002/2016GL072251.

317 Gao, X. L., Q. M. Lu, and S. Wang (2018), Statistical results of multiband chorus by
318 using THEMIS waveform data. Journal of Geophysical Research: Space Physics,
319 123, 5506–5515. https://doi.org/10.1029/2018JA025393.

320 Gao, X. L., L. J. Chen, W. Li, Q. M. Lu, and S. Wang (2019), Statistical results of the
321 power gap between lower-band and upper-band chorus waves. Geophysical
322 Research Letters, 46, 4098–4105. https://doi.org/10.1029/2019GL082140.

323 Gary, S. P., K. Liu, and D. Winske (2011), Whistler anisotropy instability at low
324 electron: Particle-in-cell simulations, Phys. Plasmas, 18(8), 082902,
325 doi:10.1063/1.3610378.

326 Huang, S. Y., et al. (2016), Two types of whistler waves in the hall reconnection
327 region, J. Geophys. Res. Space Physics, 121, 6639–6646,
328 doi:10.1002/2016JA022650.

329 Ke, Y. G., X. L. Gao, Q. M. Lu, X. Y. Wang, and S. Wang (2017), Generation of
330 rising-tone chorus in a two-dimensional mirror field by using the general
331 curvilinear PIC code. Journal of Geophysical Research: Space Physics, 122,
332 8154–8165. https://doi.org/10.1002/2017JA024178.

333 Lauben, D. S., U. S. Inan, T. F. Bell, and D. A. Gurnett (2002), Source characteristics
334 of ELF/VLF chorus, J. Geophys. Res., 107(A12), 1429,
335 doi:10.1029/2000JA003019.

336 LeDocq, M. J., D. A. Gurnett, and G. B. Hospodarsky (1998), Chorus source
337 locations from VLF Poynting flux measurements with the Polar spacecraft.
338 Geophysical Research Letters, 25(21), 4063–4066.
339 https://doi.org/10.1029/1998GL900071.

340 Li, W., R. M. Thorne, Y. Nishimura, J. Bortnik, V. Angelopoulos, J. P. McFadden, et
341 al. (2010). THEMIS analysis of observed equatorial electron distributions
342 responsible for the chorus excitation. Journal of Geophysical Research, 115,
343 A00F11. https://doi.org/10.1029/2009JA014845.

344 Li, W., J. Bortnik, R. M. Thorne, and V. Angelopoulos (2011),Global distribution of
345 wave amplitudes and wave normal angles of chorus waves using THEMIS wave

observations, J. Geophys. Res., 116, A12205, doi:10.1029/2011JA017035.

Li, W., R. M. Thorne, J. Bortnik, X. Tao, and V. Angelopoulos (2012), Characteristics of hiss-like and discrete whistler-mode emissions. Geophysical Research Letters, 39, L18106. https://doi.org/10.1029/2012GL053206.

Liu, K., S. P. Gary, and D. Winske (2011), Excitation of banded whistler waves in the magnetosphere, Geophys. Res. Lett., 38, L14108, doi:10.1029/2011GL048375.

Lu, Q. M., L. Q. Wang, Y. Zhou, and S. Wang (2004), Electromagnetic instabilities excited by electron temperature anisotropy, Chin. Phys. Lett., 21, 129-132.

Lu, Q. M., L. H. Zhou, and S. Wang (2010), Particle-in-cell simulations of whistler waves excited by an electron κ distribution in space plasma, J. Geophys. Res., 115, A02213, doi:10.1029/2009JA014580.

Meredith, N. P., R. B. Horne, and R. R. Anderson (2001), Substorm dependence of chorus amplitudes: Implications for the acceleration of electrons to relativistic energies. Journal of Geophysical Research, 106(A7), 13,165–13,178. https://doi.org/10.1029/2000JA900156.

Mourenas, D., A. V. Artemyev, O. V. Agapitov, V. Krasnoselskikh, and F. S. Mozer (2015), Very oblique whistler generation by low-energy electron streams, J. Geophys. Res. Space Physics, 120, 3665–3683, doi:10.1002/2015JA021135.

Ni, B. B., R. M. Thorne, Y. Y. Shprits, K. G. Orlova, and N. P. Meredith (2011),

Chorus-driven resonant scattering of diffuse auroral electrons in nondipolar magnetic fields. Journal of Geophysical Research, 116, A06225. https://doi.org/10.1029/2011ja016453.

Nishimura, Y., J. Bortnik, W. Li, R. M. Thorne, B. Ni, L. R. Lyons, et al. (2013). Structures of dayside whistler-mode waves deduced from conjugate diffuse aurora. Journal of Geophysical Research: Space Physics, 118, 664–673. https://doi.org/10.1029/2012JA018242.

Omura, Y., and D. Nunn (2011), Triggering process of whistler mode chorus emissions in the magnetosphere, J. Geophys. Res., 116, A05205, doi:10.1029/2010JA016280.

Omura, Y., M. Hikishima, Y. Katoh, D. Summers, and S. Yagitani (2009), Nonlinear mechanisms of lower-band and upper-band VLF chorus emissions in the magnetosphere, J. Geophys. Res., 114, A07217, doi:10.1029/2009JA014206.

Ratcliffe, H., and C. E. J. Watt (2017), Self-consistent formation of a 0.5 cyclotron frequency gap in magnetospheric whistler mode waves, J. Geophys. Res. Space Physics, 122, 8166 – 8180, doi:10.1002/2017JA024399.

Reeves, G. D., H. E. Spence, M. G. Henderson, S. K. Morley, R. H. W. Friedel, H. O. Funsten, et al. (2013), Electron acceleration in the heart of the Van Allen radiation belts. Science, 341(6149), 991–994. https://doi.org/10.1126/science.1237743.

385 Ronnmark, K. (1982). WHAMP: Waves in homogeneous, anisotropic,
386 multicomponent plasmas, Kiruna Geophysical Institute, Report 179. Kiruna,
387 Sweden.

388 Santolik, O., D. A. Gurnett, J. S. Pickett, M. Parrot, and N. Cornilleau-Wehrlin,
389 Spatio-temporal structure of storm-time chorus (2003), J. Geophys. Res.,
390 108(A7), 1278, doi:10.1029/2002JA009791.

391 Santolik, O., D. A. Gurnett, J. S. Pickett, M. Parrot, and N. Cornilleau-Wehirlin
392 (2005), Central position of the source region of storm-time chorus. Planetary and
393 Space Science, 53(1-3), 299–305. https://doi.org/10.1016/j.pss.2004.09.056.

394 Santolik, O., et al. (2010), Wave-particle interactions in the equatorial source region
395 of whistler-mode emissions, J. Geophys. Res., 115, A00F16,
396 doi:10.1029/2009JA015218.

397 Summers, D., C. Ma, N. P. Meredith, R. B. Horne, R. M. Thorne, D. Heynderickx,
398 and R. R. Anderson (2002), Model of the energization of outer-zone electrons by
399 whistler-mode chorus during the October 9, 1990 geomagnetic storm, Geophys.
400 Res. Lett. , 29 (24), 2174, doi:10.1029/2002GL016039.

401 Thorne, R. M., B. Ni, X. Tao, R. B. Horne, and N. P. Meredith (2010), Scattering by
402 chorus waves as the dominant cause of diffuse auroral precipitation. Nature,
403 467(7318), 943–946. https://doi.org/10.1038/nature09467.

Thorne, R. M., W. Li, B. Ni, Q. Ma, J. Bortnik, L. Chen, et al. (2013), Rapid local acceleration of relativistic radiation-belt electrons by magnetospheric chorus. Nature, 504(7480), 411–414. https://doi.org/10.1038/nature12889.

Tsurutani, B. T. and E. J. Smith (1974), Postmidnight chorus: A substorm phenomenon. Journal of Geophysical Research, 79(1), 118–127. https://doi.org/10.1029/JA079i001p00118.

Wang, S. M., R. S. Wang, S. T. Yao, Q. M. Lu, C. T. Russell, and S. Wang (2019), Anisotropic electron distributions and whistler waves in a series of the flux transfer events at the magnetopause. Journal of Geophysical Research: Space Physics, 124, 1753–1769. https://doi.org/10.1029/2018JA026417.

Wei, X. H., J. B. Cao, G. C. Zhou, O. Santolik, H. Re `me, I. Dandouras, N. Cornilleau-Wehrlin, E. Lucek, C. M. Carr, and A. Fazakerley (2007), Cluster observations of waves in the whistler frequency range associated with magnetic reconnection in the Earth's magnetotail, J. Geophys. Res., 112, A10225, doi:10.1029/2006JA011771.

Xiao, F. L., L. J. Chen, H. N. Zheng, and S. Wang (2007), A parametric ray tracing study of superluminous auroral kilometric radiation wave modes, J. Geophys. Res., 112, A10214, doi:10.1029/2006JA012178.

Yue, C., X. An, J. Bortnik, Q. Ma, W. Li, R. M. Thorne, G. D. Reeves, M. Gkioulidou, D. G. Mitchell, and C. A. Kletzing (2016), The relationship between the

macroscopic state of electrons and the properties of chorus waves observed by the Van Allen Probes, Geophys. Res. Lett., 43, 7804–7812, doi:10.1002/2016GL070084.

Figure captions:

Figure 1. The frequency ω/Ω_e (black lines) and linear growth rate γ/Ω_e (red lines) of whistler waves as a function of parallel wave number $k_\parallel v_{th}/\Omega_e$ for two cases with different relative drift velocities: (a) $v_d = 0$ and (b) $v_d = 1.0v_{th}$ in the high-beta regime. The solid lines indicate parallel propagating whistler waves, whereas dashed lines correspond to antiparallel propagating whistler waves, hereafter.

Figure 2. The pitch-angle distribution of electrons for (a) the case shown in Figure 1a and (b) the case shown in Figure 1b. The coded color denotes the velocity of electrons.

Figure 3. The frequency ω_d/Ω_e (black lines) and linear growth rate γ_d/Ω_e (red lines) as a function of (a, b) drift velocity v_d/v_{th}, (c, d) temperature anisotropy $T_{\perp h}/T_{\parallel h}$, and (e, f) proportion n_h/n_{total} of hot electrons. ω_d/Ω_e and γ_d/Ω_e represent the frequency and growth rate of the most unstable whistler mode in both parallel (solid lines) and antiparallel (dashed lines) directions, hereafter.

Figure 4. The frequency ω_m (black lines) and linear growth rate γ_m (red lines) as a function of wave normal angle θ for two cases with different relative drift velocities (a) $v_d = 0$ and (b) $v_d = 0.5v_{th}$ in the low-beta regime. Here, ω_m and γ_m donate the frequency and growth rate of the whistler mode with the maximum linear growth rate at each wave normal angle.

Figure 5. The pitch-angle distribution of electrons for (a) the case shown in Figure 4a

447 and (b) the case shown in Figure 4b. It has the same format as Figure 2.

448 **Figure 6.** The frequency ω_d/Ω_e (black lines), linear growth rate γ_d/Ω_e (red lines),
449 and wave normal angle θ_d (blue lines) of whistler mode as a function of (a, b, and c)
450 v_d/v_{th}, (d, e, and f) $T_{\perp h}/T_{\parallel h}$, and (g, h, and i) n_h/n_{total}. Here, θ_d represents the
451 wave normal angle of the most unstable whistler mode in both directions.

Figure 1.

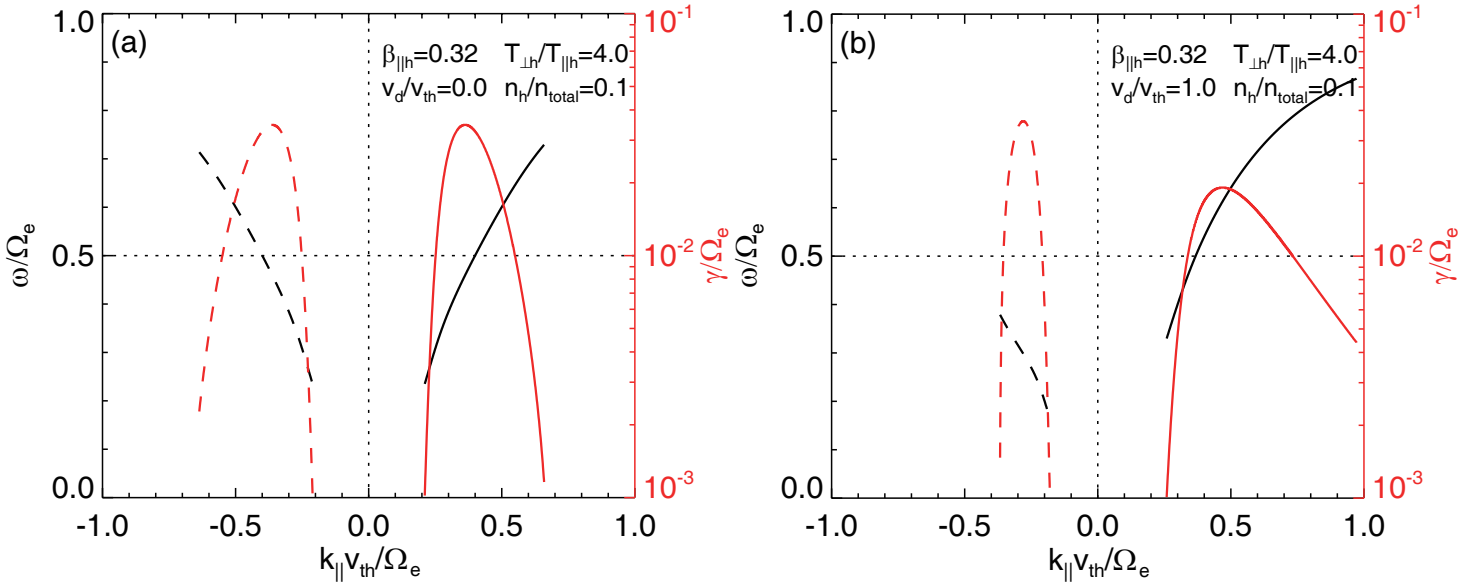
(a)
β||h=0.32 T⊥h/T||h=4.0
vd/vth=0.0 nh/ntotal=0.1
(b)
β||h=0.32 T⊥h/T||h=4.0
vd/vth=1.0 nh/ntotal=0.1
ω/Ωe
γ/Ωe
k||vth/Ωe
1.0
0.5
0.0
-1.0
-0.5
0.0
0.5
1.0
10-1
10-2
10-3

Figure 2.

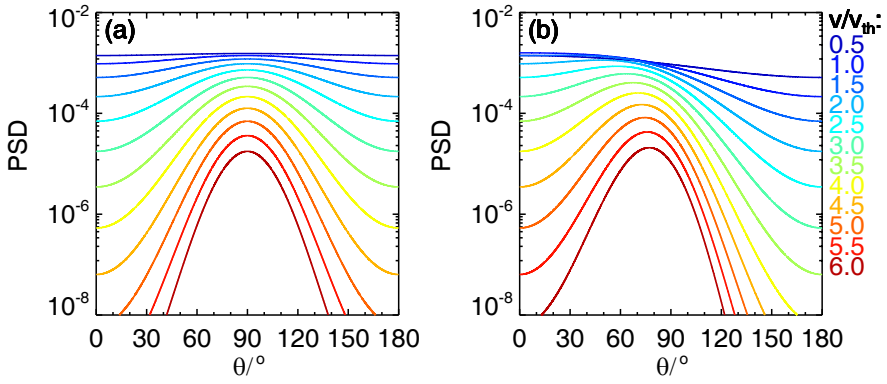
(a)
(b)
PSD
θ/°
v/v_th:
0.5
1.0
1.5
2.0
2.5
3.0
3.5
4.0
4.5
5.0
5.5
6.0

Figure 3.

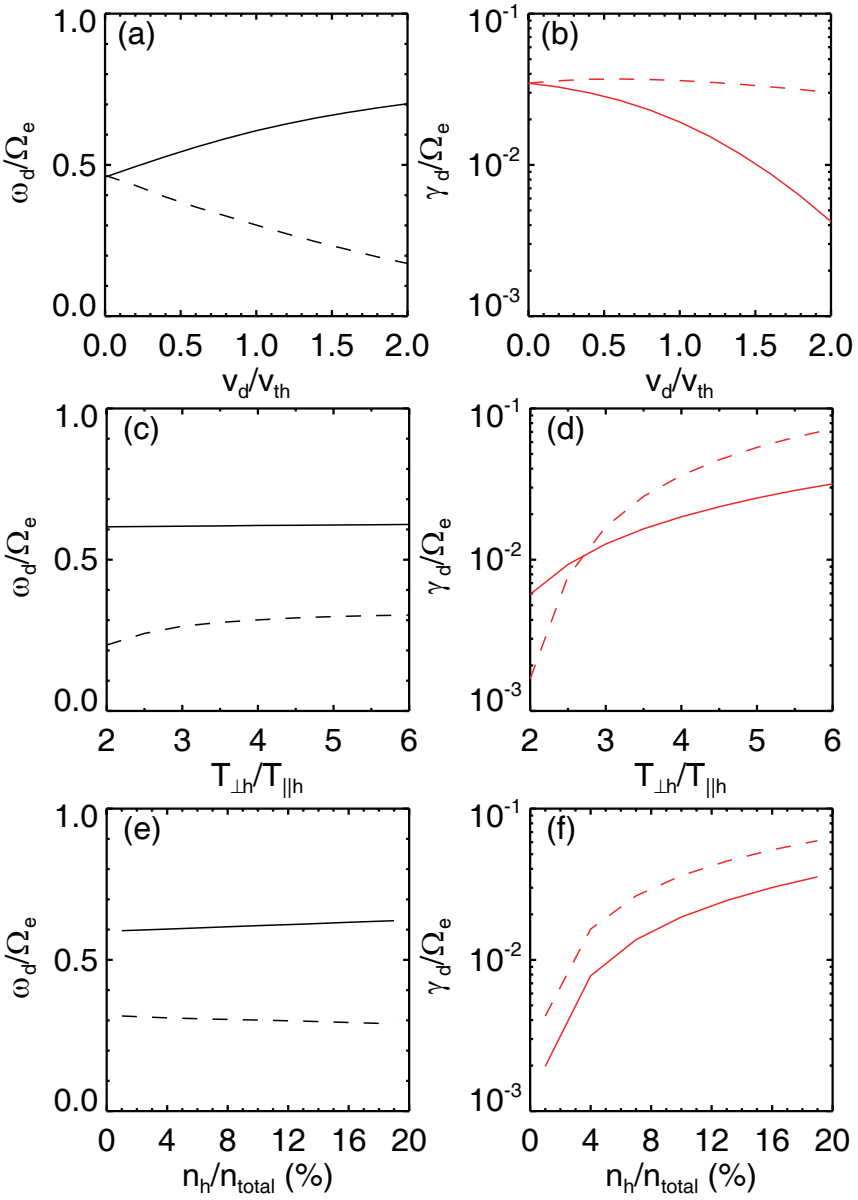
(a)
(b)
(c)
(d)
(e)
(f)
ω_d/Ω_e
γ_d/Ω_e
v_d/v_{th}
$T_{\perp h}/T_{||h}$
n_h/n_{total} (%)
1.0
0.5
0.0
10^{-1}
10^{-2}
10^{-3}
0.0 0.5 1.0 1.5 2.0
2 3 4 5 6
0 4 8 12 16 20

Figure 4.

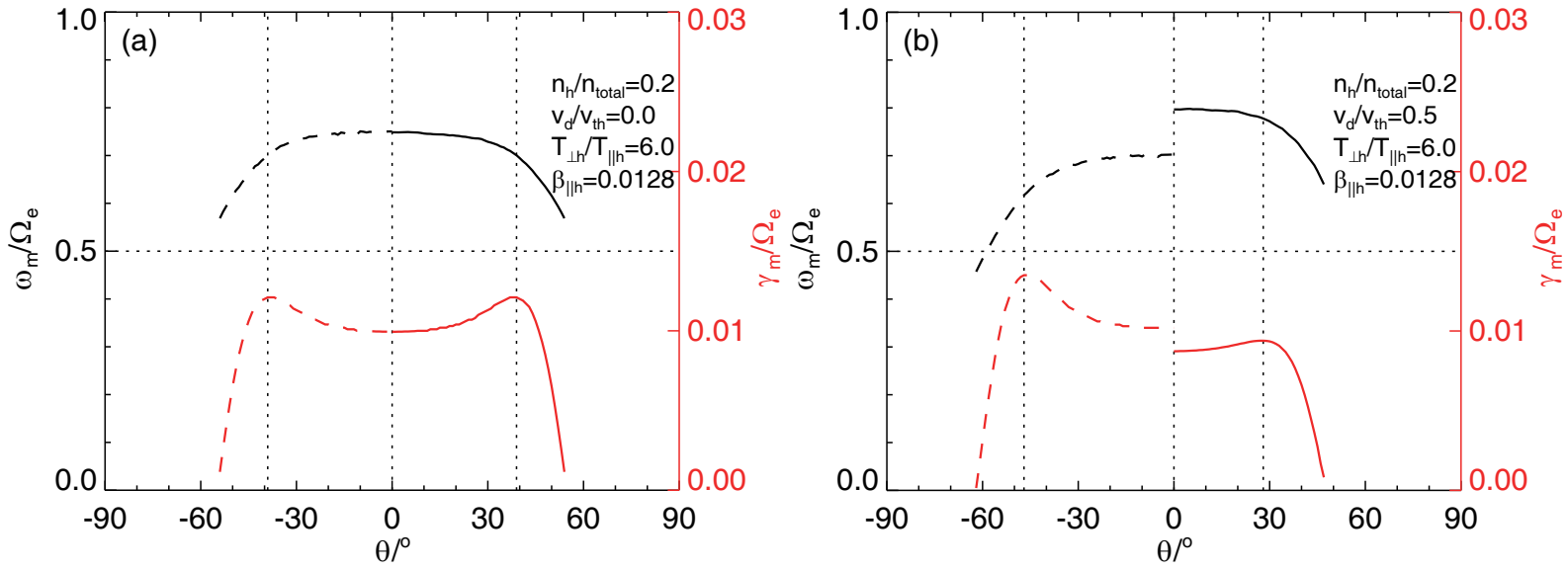
(a)
n_h/n_{total}=0.2
v_d/v_{th}=0.0
$T_{\perp h}/T_{\parallel h}$=6.0
$\beta_{\parallel h}$=0.0128
ω_m/Ω_e
γ_m/Ω_e
θ/°
(b)
n_h/n_{total}=0.2
v_d/v_{th}=0.5
$T_{\perp h}/T_{\parallel h}$=6.0
$\beta_{\parallel h}$=0.0128
ω_m/Ω_e
γ_m/Ω_e
θ/°

Figure 5.

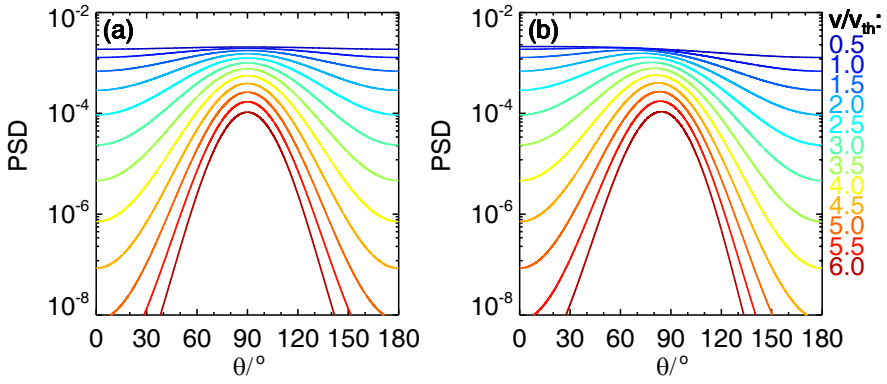
(a)
(b)
PSD
θ/°
v/v_th:
0.5
1.0
1.5
2.0
2.5
3.0
3.5
4.0
4.5
5.0
5.5
6.0

Figure 6.

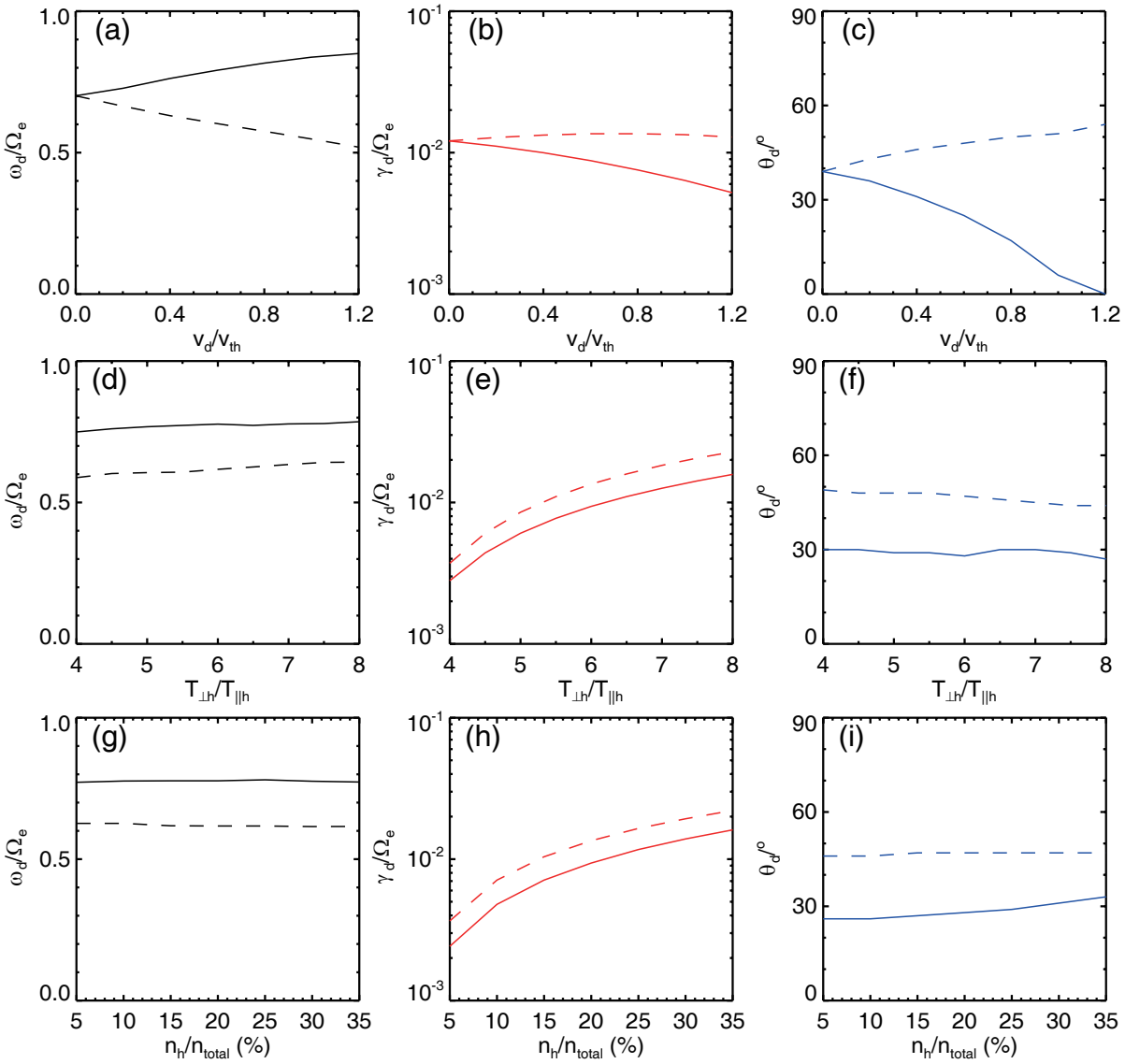
(a)
(b)
(c)
(d)
(e)
(f)
(g)
(h)
(i)
ω_d/Ω_e
γ_d/Ω_e
θ_d/°
v_d/v_{th}
$T_{\perp h}/T_{\|h}$
n_h/n_{total} (%)